Structure/activity correlation for unpromoted and CeO_2-promoted MnO_2/SiO_2 catalysts

Radu Craciun

Department of Chemical Engineering, University of Pennsylvania, 220S, 33rd Street, Philadelphia, PA 19104, USA
E-mail: rcraciun@seas.upenn.edu

Received 14 April 1998; accepted 6 August 1998

The goal of this study was to understand the structure–activity relationship for unpromoted and ceria-promoted MnO_x/SiO_2 catalysts used in CO oxidation. SiO_2 and CeO_2-promoted SiO_2 (20% CeO_2) were used as supports to prepare MnO_x/SiO_2 catalysts with various manganese (Mn) loadings. X-ray diffraction (XRD) and X-ray photoelectron spectroscopy (XPS) data indicated a higher Mn dispersion on ceria-promoted than on unpromoted MnO_x/SiO_2 catalysts. Analysis of the XRD patterns and Mn_{2p} XPS spectra indicated that Mn was present as MnO_2 on MnO_x/SiO_2 with low Mn loadings and ceria-promoted MnO_x/SiO_2 catalysts and as mixed MnO_2/Mn_2O_3 on MnO_x/SiO_2 catalysts with high Mn loadings. Kinetic data obtained for CO oxidation on unpromoted and ceria-promoted MnO_x/SiO_2 catalysts are presented and interpreted in correlation with the catalyst surface and bulk structure. A synergistic catalytic effect was observed in the case of the ceria-promoted MnO_x/SiO_2 catalysts. Post-reaction XRD and XPS analysis of catalysts indicated that the presence of ceria precludes formation of the less catalytically active Mn_3O_4 species from MnO_2 deposited initially on the SiO_2 support.

Keywords: ceria promoter, manganese oxides, silica, CO oxidation, synergism

1. Introduction

Manganese oxide (MnO_2) is used as the active phase in several catalytic oxidation processes such as CO oxidation [1,2], oxidative coupling of methane [3,4], ethylbenzene oxidative dehydrogenation [5] as well as other types of catalytic processes [6–17]. In general, manganese oxides have a typical berthollide structure that contains labile lattice oxygen. Their catalytic properties are attributed to the variability of the Mn oxidation state allowing formation of oxides with a variety of stoichiometries (MnO_2, Mn_2O_3, Mn_3O_4, or MnO) and to their oxygen storage capacity in the crystalline lattice. Structural characterization of unsupported or supported MnO_x catalysts has identified the presence of MnO_2 or mixed MnO_2/Mn_2O_3 as the active catalytic components [5,14,16]. The ratio between the MnO_2 and Mn_2O_3 phases is a function of the manganese loading and the catalyst calcination temperature during preparation [14,16,17]. An increased dispersion of the MnO_x on the support surface leads to significant increases in catalytic activity; this has been attributed to higher catalyst surface exposed to the reaction feed [1,15–17]. The MnO_2 dispersion depends on Mn precursor, loading, preparation method, presence of promoters and post-preparation thermal treatment [5,17].

Combinations of two elements deposited on a given support and used as catalysts in catalytic oxidation processes exhibit different catalytic activity as compared to a single component catalyst. The interaction of Mn with the support as well as with other components present in the catalyst, significantly influences its bulk and surface structure [5,11]. Previous studies have shown that when MnO_2 is placed in the proximity of La_2O_3 or CeO_2, the oxygen mobility from the MnO_x structure is strongly affected [17,18]. Based on catalytic activity data from CO oxidation and N_2O decomposition and thermogravimetric analysis, it is believed that in Mn–Ce mixed oxides catalysts, Ce can provide oxygen to Mn at low temperature and withdraws oxygen at elevated temperatures ($>500\,^{\circ}C$) [18]. Thus, cerium improves the activity of MnO_x in oxidation processes at lower temperature and decreases its activity at high temperature, the active component in this case being CeO_2 which takes oxygen away from MnO_x [18].

The interest in the study of MnO_x-based catalysts is an indication of their importance in the chemical industry, particularly in selective oxidation and oxidative dehydrogenation processes. Despite the considerable effort devoted to the study of Mn-based catalysts, identification of the active sites, the role of promoters, mixed oxide effects, and the structure of any surface phases are still the subject of many controversies. This work is directed toward understanding the relationship which exists between the structure of the unpromoted and ceria-promoted MnO_x supported on high surface area SiO_2 and their catalytic activity. Surface and bulk structural information, for the $MnO_x/CeO_2/SiO_2$ catalysts has been obtained using X-ray diffraction (XRD) and X-ray photoelectron spectroscopy (XPS). Kinetic data and the proposed reaction mechanism for CO oxidation on unpromoted and ceria-promoted MnO_x/SiO_2 are presented in correlation with the surface and bulk structure of the catalysts.

2. Experimental

2.1. Catalysts preparation

Three different supports were used for MnO_x catalysts preparation; unpromoted SiO_2 and two types of CeO_2-promoted SiO_2 obtained by impregnation with Ce^{4+}-nitrate (CeN) and with Ce^{4+}-methoxyethoxide (CeA). Details about preparation of the support are given elsewhere [19]. MnO_x supported catalysts were prepared using aqueous manganese nitrate $Mn(NO_3)_2{\cdot}6H_2O$ (Aldrich) precursors by wet impregnation. The Mn content was chosen to be 12 wt% (Mn12N) and 23 wt% (Mn23N) MnO_2 relative to the support. The CeO_2-promoted MnO_x/SiO_2 catalysts were prepared by sequential impregnation (Ce followed by Mn) and were designated as Mn12CeN (for CeN support) and Mn12CeA (for CeA support). All samples were dried at 125 °C and calcined for 16 h in air at 500 °C after each impregnation step, prior to using them in the CO oxidation process.

2.2. Structure analysis

Surface area measurements were performed using a Quanta-Chrome Quantasorb Jr. Sorption System. Approximately 0.1 g of catalyst was outgassed in N_2 at 165 °C for 12 h, prior to adsorption measurements. The measurements were made using N_2 partial pressures in He of 0.05, 0.08, and 0.15 Torr (N_2 surface area = 0.162 nm^2) at liquid N_2 temperature (77 K). The estimated error for the S_a results is ±5%. X-ray powder diffraction patterns (XRD) were obtained with a Rigaku XRD diffractometer employing Cu Kα radiation ($\lambda = 1.541838$ Å) and operated at 45 kV and 100 mA. The mean crystallite size ($\bar{d}$) of the MnO_x samples was determined from XRD line broadening calculations, using the Scherrer equation: $\bar{d} = k\lambda/\beta\cos\theta$, where λ is the X-ray wavelength, k is the particle shape factor (here, 0.9 for cubic particles), β is the full width at half maximum (FWHM) in radians, and θ is the diffraction angle [20]. XRD patterns for various MnO_x and CeO_2 phases were identified by comparing the experimental results with those from the XRD data base [21]. X-ray photoelectron spectroscopy (XPS) data were obtained using a Perkin-Elmer Surface Science instrument equipped with a magnesium anode (1253.6 eV) operated at 300 W (15 kV, 20 mA) and a 10–360 hemispherical analyzer operated with a pass energy of 50 eV. Spectra were collected using a PC137 board interfaced to a Zeos 386SX computer. Samples were analyzed as powders dusted on tape. Binding energies for the catalyst samples were referenced to the Si_{2p} peak (103.4 eV). XPS binding energies were measured with a precision of ±0.2 eV or better.

2.3. Activity measurements

CO oxidation was used to test the catalytic activity of the unpromoted and ceria-promoted MnO_x/SiO_2 catalysts. Rates for CO oxidation were measured by placing the thin catalyst pellets into a quartz tubular reactor. The total pressure in the reactor was maintained at atmospheric pressure. Air was used as the oxidant and helium as the carrier gas. The reaction was carried out with $p_{CO} = 5$ Torr and $p_{O_2}/p_{CO} = 1.1$. Differential conditions were maintained for all measurements, the CO conversions being typically less than 10%. Activation energies are evaluated from the slope of the Arrhenius plots. Rates were highly reproducible and remained constant over a period of several hours. Product analysis (CO_2 and CO) was performed with an on-line HP-5730A gas chromatograph, equipped with a methanator and FID detector. All the reported rates were normalized to the weight of the catalyst pellet.

3. Results

3.1. Catalysts characterization

The BET surface areas of the unpromoted and CeO_2-promoted MnO_x/SiO_2 catalysts are presented in table 1. The surface area of SiO_2 support was evaluated to be 300 m^2/g. MnO_x and CeO_2 have negligible surface areas compared to SiO_2. Consequently, the small variations observed in the surface area are due to a weight effect from

Table 1
Characterization data for unpromoted and ceria-promoted MnO_x/SiO_2 catalysts.

Catalyst	S_a (m^2/g)	$\bar{d}$ [a] MnO_2 (nm)	$Mn_{2p_{3/2}}$ BE [b] (eV)		XPS [c] $I_{Mn_{2p}}/I_{Si_{2p}}$	E_a
			Fresh	Used	corrected	(kcal/mol)
Mn23N	255	16.5	642.5 (640.8)	640.7 (642.6)	1.08	28.8
Mn12N	257	15.5	642.4	640.7 (642.6)	0.98	11.7
Mn12CeA	225	6.7	642.3	642.4	1.77	9.8
Mn12CeN	230	13.8	642.3	642.3	1.13	9.3
CeA	300	–	–	–	–	14.9
CeN	303	–	–	–	–	13.2

[a] Evaluated from XRD line broadening calculations.
[b] The values in parentheses are the BE of the deconvoluted peaks which appeared as a shoulder to the main and most intense peaks from the XPS $Mn_{2p_{3/2}}$ spectra.
[c] Evaluation of XPS $I_{Mn_{2p}}/I_{Si_{2p}}$ ratio based on corrected area using the atomic sensitivity factor of Mn and Si specific to the instrument.

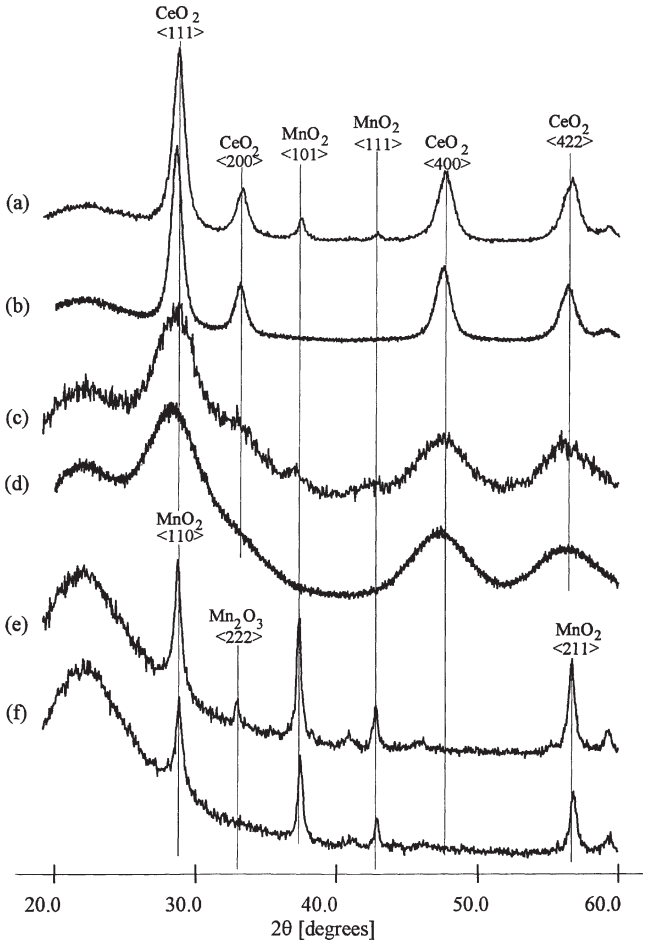

Figure 1. XRD patterns of unpromoted and CeO_2-promoted MnO_x/SiO_2 catalyst: (a) Mn12CeN, (b) CeN, (c) Mn12CeA, (d) CeA, (e) Mn23N, (f) Mn12N.

the MnO_x and CeO_2 phases present on the high surface area SiO_2 support.

The crystallinity and particle size of unpromoted and ceria-promoted MnO_x/SiO_2 catalysts were estimated from XRD data (figure 1). In the case of unpromoted MnO_x/SiO_2 catalysts the XRD data (figure 1, spectra (e) and (f)) indicated that after impregnation with Mn-nitrate precursor and calcination at 500 °C, MnO_2 and Mn_2O_3 were readily formed on the support. According to the XRD data (figure 1), a Mn_2O_3 phase was formed only on the Mn23N catalysts. The differences in MnO_2 particle size (table 1) for the unpromoted MnO_x/SiO_2 catalysts considered in this study were small. The Mn dispersion can be evaluated from the XPS $I_{Mn_{2p}}/I_{Si_{2p}}$ values as well (table 1). Previous studies have shown that Mn dispersion varies with Mn loading, pretreatment temperature of the catalyst, and the presence of promoters [5,17,21]. Low values of $I_{Mn_{2p}}/I_{Si_{2p}}$ for unpromoted MnO_x/SiO_2 (e.g., 0.98 for Mn23N) are indicative of poor Mn dispersion on high surface area SiO_2. The small differences observed in $I_{Mn_{2p}}/I_{Si_{2p}}$ for the Mn12N catalyst (1.08) compared with Mn23N (0.98) which is indicative of comparable MnO_2 dispersion, are consistent with comparable particles size as calculated from XRD line broadening. The BE values for $Mn_{2p_{3/2}}$ are presented in table 1. For the Mn12N catalyst, the symmetric peak located at 642.4 eV indicates the presence of Mn as Mn^{4+} in MnO_2. For the Mn23N catalyst, the asymmetric peak, deconvoluted in two separate peaks located at 642.5 and 640.8 eV, indicates the existence of Mn as a mixed Mn^{4+}/Mn^{3+} phase from MnO_2 and Mn_2O_3. These data are in good agreement with the XRD results presented in figure 1 (e) and (f) which show mixed patterns of these types of manganese oxides [17,21].

The XRD spectra of CeO_2-promoted MnO_2/SiO_2 catalysts are presented in figure 1 (a) and (c). The XRD spectra of the ceria-promoted silica supports are shown for reference in figure 1 (b) and (d), respectively. Analysis of the XRD spectra of CeO_2/SiO_2 indicate a variation in the ceria dispersion and crystallinity. The main difference between the two ceria-promoted supports is the size of the ceria crystallites, 2.5 nm on CeA support compared to 10 nm on the CeN support. For the CeO_2-supported MnO_x/SiO_2 catalysts (figure 1 (a) and (c)), diffuse and broad XRD patterns specific to a MnO_x crystalline phase together with XRD patterns specific to CeO_2 were observed. This can be attributed either to formation of small MnO_x particles or to an amorphous Mn phase on the CeO_2-promoted SiO_2 catalysts calcined at 500 °C. Analyzing the positions of the diffuse XRD patterns other than those specific to CeO_2, indicates that the most probable Mn species formed in these cases is MnO_2. It seems that the presence of ceria favors MnO_2 dispersion on the SiO_2 support. The particle size of MnO_2 on Mn12CeA and Mn12CeN catalysts is presented in table 1 together with BET surface areas and XPS data. For Mn12CeA catalysts the mean crystalline particle size ($\bar{d}$) of MnO_2 was 6.7 nm, significantly lower than that observed for MnO_2 on Mn12CeN (13.8 nm) or on Mn12N (15.5 nm) catalysts. This fact can probably be attributed to an interaction between the CeO_2 promoter and MnO_2 during impregnation and calcination, which favored formation of small MnO_2 crystallites. For both types of ceria-promoted catalysts, the XPS spectra of $Mn_{2p_{3/2}}$ show a symmetric peak located at 642.2 eV, characteristic to Mn^{4+} from MnO_2. The XPS dispersion data presented in table 1 show a higher $I_{Mn_{2p}}/I_{Si_{2p}}$ intensity ratio for Mn12CeA (1.77) or Mn12CeN (1.13) catalysts as compared to that for unpromoted Mn12N (1.08) and Mn23N (0.98) catalysts, indicating a better Mn dispersion on the ceria-promoted catalysts.

3.2. Catalytic activity

Figure 2 shows Arrhenius plots for the CO oxidation on unpromoted and ceria-promoted MnO_2/SiO_2 catalysts. As observed, the CO oxidation rates on Mn12N or Mn23N catalysts are situated around 8×10^{16} molecules/s g_{cat} at 200 °C. The results show an increase in the CO conversion rates with higher Mn loadings. The rates on CeA catalysts are higher (doubled) than those obtained on CeN catalysts and are situated around the same values as those recorded for Mn12N catalysts. A significant increase in

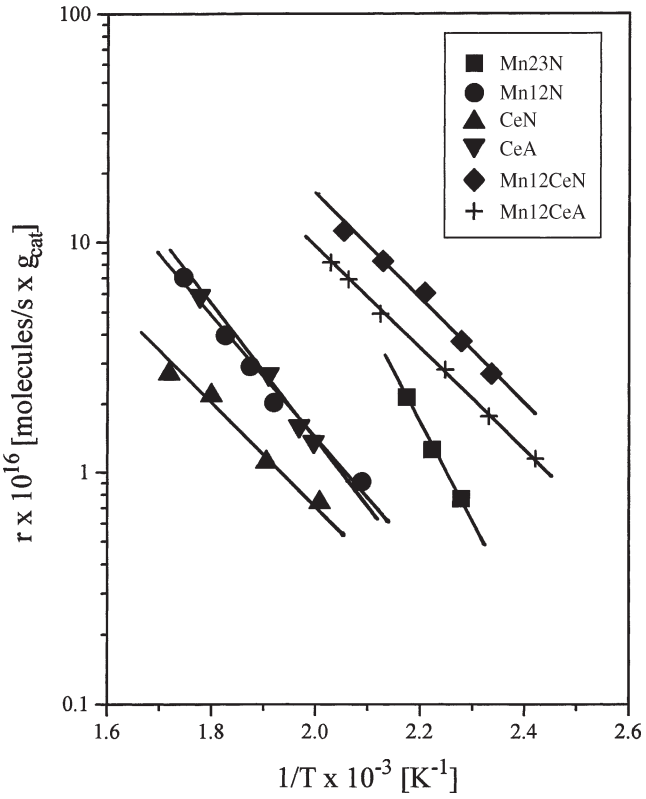

Figure 2. Arrhenius plots from CO oxidation: Mn23N (■), Mn12N (●), CeN (▲); CeA (▼), Mn12CeN (♦), and Mn12CeA (+) catalysts.

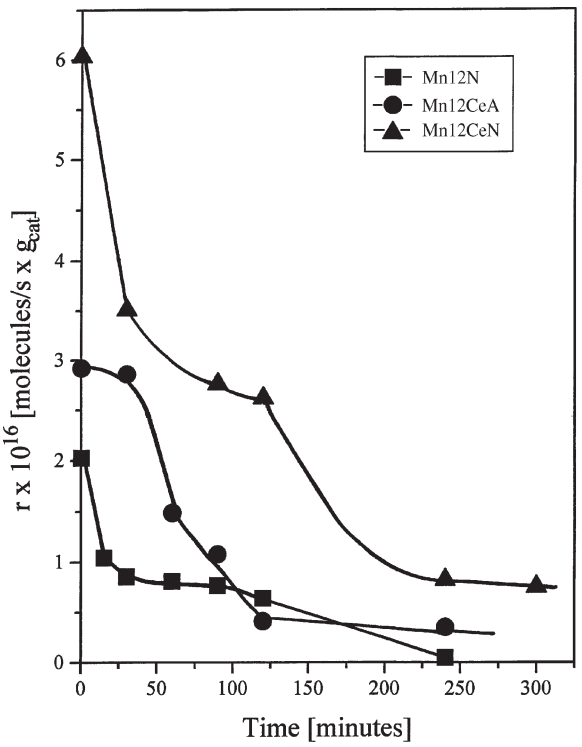

Figure 3. Transient experiment data obtained for Mn12N (■), at 248 °C, Mn12CeA (●) 180 °C, and Mn12CeN (▲) 180 °C catalysts.

reaction rate was observed on ceria-promoted MnO_2 catalysts, where they are an order of magnitude higher than those recorded for unpromoted Mn12N catalysts (same Mn loading, 12% MnO_2) or plain ceria-promoted SiO_2 support. This observation implies a synergistic effect between MnO_2 and CeO_2, where probably one component provides the adsorption site for CO and the other provides a continuous source of oxygen necessary for oxidation. The activation energies (see table 1) determined from the data presented in figure 2 are around 9–14 kcal/mol (except for Mn23N catalyst), close to values previously reported in the literature [25–27]. A good MnO_2 or CeO_2 dispersion determines an efficient and intimate contact between the reactants (CO) and the active sites from the catalyst surface, favoring the product formation (CO_2). The neat SiO_2 support shows the negligible activity for CO oxidation, the rates being less than 1×10^{14} molecules/s g_{cat} at 240 °C.

Further information about the kinetics and mechanism of CO oxidation on ceria-promoted MnO_2/SiO_2 catalysts were obtained from transient experiments data. Figure 3 shows the variation in CO oxidation rates obtained on Mn12N at 248 °C, and Mn12CeN and Mn12CeA at 180 °C as a function of the time elapsed after the air supply was discontinued. Due to extremely low reaction rates at 180 °C on Mn12N catalysts, the experiments had to be performed at 248 °C. For all catalysts the rate of CO oxidation decreased significantly after 120 min. Compared to Mn12N catalyst, both types of ceria-promoted catalysts (Mn12CeN and Mn12CeA) show higher catalytic activity (higher rates) at lower temperature for longer time after the source of oxygen was removed. For all catalysts, for a short period of time it appears that the oxygen for CO oxidation can be provided by the lattice oxygen of the supported metal oxides. This effect is more pronounced when the ceria-promoter is present on the catalyst surface.

3.3. Used catalysts

The used catalysts from CO oxidation were analyzed by XRD and XPS. Diffraction patterns obtained for these catalysts are presented in figure 4. In the case of the used Mn12N catalyst, new peaks are observed (figure 4(a)) compared to those for the fresh catalyst (see figure 1(f)). These patterns were identified based on literature data and analysis of reference compounds; they were attributed to Mn_3O_4 ($MnO{\cdot}Mn_2O_3$) species formed during the catalytic process [21]. In the oxidation reaction, MnO_x species act as oxygen donors, and consequently, are reduced to Mn_3O_4. It was observed that MnO_2 can be regenerated by recalcination at 500 °C in air. The XRD spectra of used CeO_2-promoted MnO_x/SiO_2 catalysts are presented in figure 4 (b) and (c), respectively. Compared with the fresh catalysts (see figure 1 (a) and (c)), the XRD patterns of the used catalysts remain mostly unchanged. However, traces of XRD peaks specific to Mn_3O_4 species are observable in the case of the Mn12CeN catalyst (figure 4(b)), whereas they are absent in the XRD patterns of the Mn12CeA catalyst (figure 4(c)). It appears that the presence of ceria affects the resistance of MnO_2 to reduction during the cat-

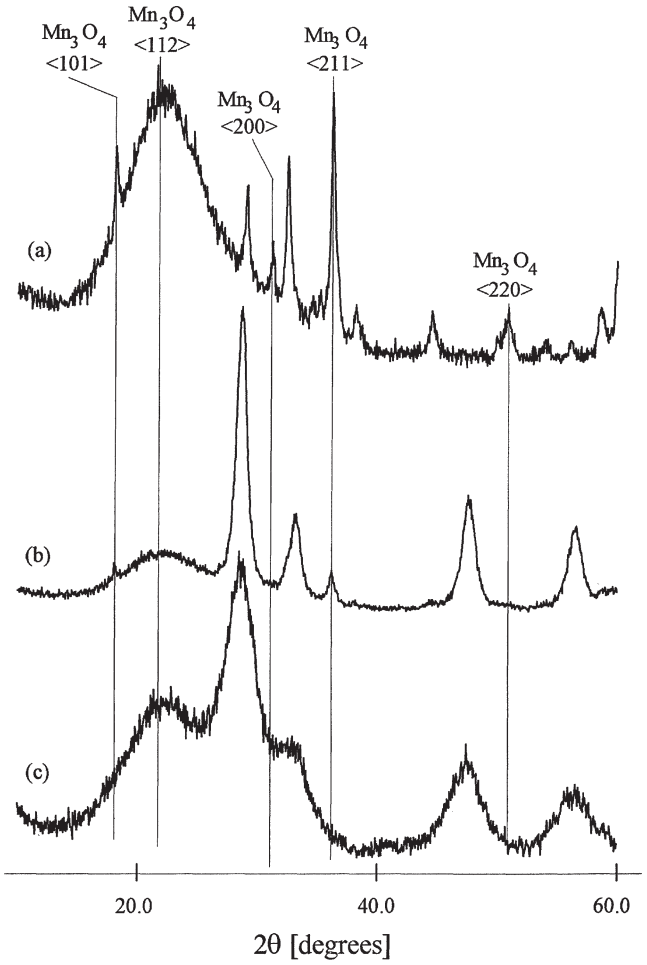

Figure 4. XRD patterns of used unpromoted and CeO_2-promoted catalysts: (a) Mn12N, (b) Mn12CeN, (c) Mn12CeA.

alytic process, being able to provide oxygen to Mn and maintain its oxidation state unchanged.

The $Mn_{2p_{3/2}}$ XPS spectrum for used Mn12N catalyst displays a shift in BE from 642.5 eV, a value characteristic to Mn as Mn^{4+}, to 640.8 eV, a value characteristic to Mn as Mn^{3+} or Mn^{2+} (table 1). Literature data show that the BE for $Mn_{2p_{3/2}}$ in Mn_3O_4 is situated between 641.3–641.4 eV, and for Mn_2O_3 species between 641.3–641.9 eV [17,28]. Hence, it is hard to identify a signal specific to Mn^{2+} when it is mixed with Mn^{3+} due to the overlap of their peaks and relatively close BE values. For the ceria-promoted MnO_2/SiO_2 catalysts the BE for $Mn_{2p_{3/2}}$ reported in table 1 is 642.5 ± 0.2 eV. This corresponds to Mn^{4+} from MnO_2 and is similar to the value obtained for the fresh catalyst. The $Mn_{2p_{3/2}}$ peak for the Mn12CeN catalyst shows a small degree of asymmetry which might indicate the traces of Mn^{3+} and Mn^{2+}. Despite the low S/N of the $Mn_{2p_{3/2}}$ XPS spectra, the results are in good agreement with those obtained from XRD, that also show peaks specific to Mn_3O_4. The $Mn_{2p_{3/2}}$ XPS spectrum for used Mn12CeA catalysts shows that the major peak is located at 642.5 eV and corresponds to Mn^{4+}. This indicates that Mn is present most probably as MnO_2.

4. Discussion

For Mn12N catalysts, the XRD and XPS results indicated the formation of MnO_2 phase with particles around 15.5 nm in diameter, after air calcination at 500 °C. Thus, during calcination, Mn^{2+} is easily oxidized to Mn^{4+} forming only a crystalline MnO_2 phase. In the case of Mn23N catalysts, Mn is probably forming large clusters of $Mn(NO_3)_2$ less accessible to oxygen, during the impregnation and drying process. Consequently, the oxidation of $Mn(NO_3)_2$, which occurs during drying (H_2O removal) and air calcination (NO_2 elimination) led to formation of both MnO_2 and Mn_2O_3 phases (observed as large crystallites on the SiO_2 surface). Because of the small difference observed in the MnO_2 particle size between Mn12N and Mn23N catalysts, the variation in reaction rates shown in figure 2 can be correlated to the Mn loading (higher rates for higher Mn loadings). The activation energies calculated differs significantly, 11.7 kcal/mol for Mn12N compared to 28.8 for Mn23N. This fact can be attributed to the higher amount of Mn_2O_3 phase present in the Mn23N catalyst, which is less catalytically active. Hence, probably in the first step, Mn_2O_3 is transformed into MnO_2 (reaction (4)), which in the second step catalyses the reaction. Both Mn12N and Mn23N catalysts show formation of Mn_3O_4 species after exposure to the reaction feed (CO), leading to a decrease in time of their catalytic activity. Hence, the oxidation of CO probably occurs by the following mechanism:

$$CO_{ads} + 2MnO_2 \rightarrow CO_2 + Mn_2O_3 \quad (1)$$

$$CO + MnO_2 + Mn_2O_3 \rightarrow CO_2 + Mn_3O_4 \quad (2)$$

$$Mn_3O_4 + O_2\ (\text{air}) \rightarrow MnO_2 + Mn_2O_3 \quad (3)$$

$$Mn_2O_3 + (1/2)O_2\ (\text{air}) \rightarrow 2MnO_2 \quad (4)$$

The presence of CeO_2 on the MnO_x/SiO_2 catalysts precludes the formation of Mn_3O_4 species during exposure to reaction conditions, conferring a stronger oxidation power (high rates, figure 2), lower activation energies (see table 1), and resistance to deactivation to the catalysts. This effect is more significant in the case of the Mn12CeA catalyst, probably due to a stronger Mn–Ce interaction. The more stable MnO_2 on the ceria-promoted MnO_2/SiO_2 catalysts can be related to the ability of ceria to provide lattice oxygen to Mn_2O_3 or Mn_3O_4. MnO_2 is regenerated while the Ce_2O_3 can be readily reoxidized by air to CeO_2.

Thus, the proposed mechanism in this case is as follows:

$$CO_{ads} + 2MnO_2 \rightarrow CO_2 + Mn_2O_3 \quad (1)$$

$$Mn_2O_3 + 2CeO_2 \rightarrow 2MnO_2 + Ce_2O_3 \quad (5)$$

$$Ce_2O_3 + (1/2)O_2\ (\text{air}) \rightarrow 2CeO_2 \quad (6)$$

This mechanism explains the ceria promotion effect and the synergistic effect observed from the activity data (figure 2, crosses and diamonds) for ceria-promoted MnO_2/SiO_2 catalysts. A similar effect was previously observed for noble metals (Rh, Pd, Pt) supported on ceria [26,27]. In this case, adsorbed CO on active sites from the noble metal surface are oxidized by ceria lattice oxygen

with the formation of Ce_2O_3. It is well known that Ce_2O_3 can be easily reoxidized to CeO_2 by exposure to air or H_2O vapors [25,26]. In this case, CO is oxidized by the lattice oxygen of MnO_2 followed by oxygen migration from ceria to regenerate the Mn catalyst.

On both types of used CeO_2-promoted MnO_x/SiO_2 catalysts, Mn remains well dispersed on high surface area supports, with a structure similar to that of the fresh catalyst. The activation energy on both types of ceria-promoted catalysts is ≈9 kcal/mol, smaller than that calculated for Mn12N and CeA (N) catalysts (close to 13 kcal/mol, see table 1). Smaller MnO_2 crystallites, lower catalytic activity, and no Mn_3O_4 phase formation on Mn12CeA compared to Mn12CeN catalysts suggests the possibility of $MnCeO_x$ mixed oxide formation with less accessible Mn sites, either to CO molecules or to air [19]. In the case of the Mn10CeN catalyst, MnO_x deposits coexist in intimate contact with CeO_2 crystallites (probably just as a physical mixture) favoring oxygen transfer between the two metal oxides. This type of MnO_2–CeO_2 structure/interaction leads to high catalytic activity and formation of small amounts of a Mn_3O_4 phase. The formation of Mn_3O_4 on Mn12CeN catalysts can be explained by considering the formation of "islands" of MnO_2 and CeO_2, without any interaction between them, which allows the formation Mn_3O_4 from MnO_2 in the absence of ceria interaction. For both types of ceria-promoted MnO_2/SiO_2 catalysts, transient experiments indicate a stronger oxidation power, the catalysts remaining active for longer time in comparison with the unpromoted MnO_2/SiO_2 catalysts. Again, this fact can be attributed to the ability of ceria to provide oxygen to MnO_2 which finally oxidizes the CO to CO_2. These data support the proposed mechanism for CO oxidation on unpromoted and ceria-promoted MnO_2/SiO_2 catalysts (reactions (1)–(6)).

5. Conclusions

XRD and XPS analysis of unpromoted MnO_2 supported on high surface area SiO_2 indicated that Mn was present in mixed MnO_2/Mn_2O_3 crystalline phases on catalysts with high Mn loading (23%) and as a single MnO_2 phase on catalysts with low Mn loading (12%). The reaction rates for catalytic CO oxidation were proportional to Mn loading and were near 8×10^{16} molecules/s g_{cat} at 200 °C. Analysis of the used catalysts showed that the Mn oxidation state changes from Mn^{4+} to Mn^{2+}, by providing oxygen to the reactants (CO) and thus leading to the formation of the less active Mn_3O_4 species. The formation of Mn_3O_4 might be responsible for the decrease in the catalytic activity of the unpromoted MnO_x catalysts.

The presence of CeO_2 favors the dispersion of the manganese oxides deposited on the SiO_2 catalyst during calcination. Manganese was present as MnO_2 species on the fresh ceria-promoted MnO_2/SiO_2 catalysts. The rates observed in the catalytic CO oxidation are an order of magnitude higher (9×10^{17} molecules/s g_{cat}) than those recorded on unpromoted or just ceria-promoted SiO_2 catalysts. This observation suggests a synergistic effect between MnO_2 and CeO_2 similar to that previously observed for noble metals supported on ceria catalysts [26,27]. The ceria dispersion on the high surface area silica plays only a minor role in the catalytic activity of MnO_2. The presence of CeO_2 on the MnO_x/SiO_2 catalysts precludes the formation of Mn_3O_4 species during the catalysis process, conferring to the catalysts a stronger oxidation power and resistance to deactivation.

Acknowledgement

The author is grateful for the assistance of Dr. James E. Jackson and Dr. Simon Garrett from Chemistry Department at Michigan State University and of Dr. Raymond J. Gorte and Dr. John M. Vohs from Chemical Engineering Department at University of Pennsylvania for the useful discussions and suggestions after reviewing this manuscript.

References

[1] J. Mooi and P.W. Selwood, J. Am. Chem. Soc. 74 (1952) 2461.
[2] A.K.H. Nohman, D. Duprez, C. Kappenstein, S.A.A. Mansour and M.I. Zaki, in: *Preparation of Catalysts V*, eds. B. Delmon, P.A. Jacobs and G. Poncelet (Elsevier, Amsterdam, 1991) p. 617.
[3] R. Burch, S. Chalker, G.D. Squire and S.C. Tsang, J. Chem. Soc. Faraday Trans. 86 (1990) 1607.
[4] J. Wu, S. Li, J. Niu and X. Fang, Appl. Catal. 124 (1995) 9.
[5] R. Craciun and N. Dulamita, Catal. Lett. 46 (1997) 229.
[6] M.A. Baltanas, A.B. Stiles and J.R. Katzer, Appl. Catal. 28 (1986) 13.
[7] T. Yamashita and A. Vannice, J. Catal. 163 (1996) 158.
[8] A. Nishino, Catal. Today 10 (1991) 107.
[9] G.D. Moggridge, T. Rayment and R.M. Lambert, J. Catal. 134 (1992) 242.
[10] L.S. Singoredjo, R.B. Korver, F. Kapteijn and J.A. Moulijn, Appl. Catal. 1 (1992) 297.
[11] A. Wollner, F. Lange, H. Schmetz and H. Knözinger, Appl. Catal. 94 (1993) 181.
[12] T. Akiyama, Y. Enomoto and T. Shibamoto, J. Agric. Food Chem. 26 (1978) 1176.
[13] F. Kapteijn, L. Singoredjo, M. van Driel, A. Andreini, J.A. Moulijn, G. Ramis and G. Busca, J. Catal. 150 (1994) 105.
[14] X. Longya, W. Quigxia, X. Yide and H. Jiashng, Catal. Lett. 31 (1995) 253.
[15] B.R. Strohmeier and J. Hercules, J. Phys. Chem. 88 (1984) 4922.
[16] S. Cavallaro, N. Bertuccio, P. Antonucci and N. Giordano, J. Catal. 73 (1982) 337.
[17] F. Kapteijn, D. van Langeveld, J.A. Moulijn, A. Andreini, M.A. Vuurman, A.M. Turek, J.M. Jehng and I.E. Wachs, J. Catal. 150 (1994) 94.
[18] S. Imamura, M. Shono, A. Okamoto and S. Ishida, Appl. Catal. 142 (1996) 279.
[19] (a) R. Craciun, Solid State Ionics (1998), in press;
(b) R. Craciun, Ph.D. thesis, Department of Chemistry, Michigan State University, East Lansing (1997).
[20] H.P. Klug and L.E. Alexander, *X-ray Diffraction Procedures for Polycrystalline and Amorphous Materials*, 1st Ed. (Wiley, New York, 1954).
[21] W.F. McClune, Powder diffraction file, Inorganic phases, International Center for Diffraction Data, Swarthmore, 23–24 (1983) 730, 731.

[22] M.A. Baltanas, A.B. Stiles and J.R. Katzer, J. Catal. 88 (1984) 362.
[23] E. Abi-Aad, A. Bennani, J.P. Bonnelle and A. Aboukais, J. Chem. Soc. Faraday Trans. 91 (1995) 99.
[24] M. Shelef, L.P. Haack, R.E. Soltis, J.E. DeVries and E.M. Logothetis, J. Catal. 137 (1992) 114.
[25] A. Trovarelli, Catal. Rev. 38 (1996) 439.
[26] (a) T. Bunluesin, H. Cordatos and R.J. Gorte, J. Catal. 157 (1995) 222;
(b) T. Bunluesin, R.J. Gorte and G.W. Graham, Appl. Catal. 14 (1997) 105.
[27] (a) H. Cordatos, T. Bunluesin, J. Stubenrauch, J.M. Vohs and R.J. Gorte, J. Phys. Chem. 100 (1996) 785;
(b) R. Craciun, B. Shereck and R.J. Gorte, Catal. Lett. 51 (1998) 149.
[28] J.K. Moulder, W.F. Stickle, P.E. Sobol and K.D. Bomben, *Handbook of X-ray Photoelectron Spectroscopy* (Perkin-Elmer, Eden Prairy, 1992) p. 40.